2020

Numerical Modelling of Track Behavior Capturing Particle Breakage under Dynamic Loading

Ngoc Trung Ngo
University of Wollongong, trung@uow.edu.au

Buddhima Indraratna
University of Wollongong, indra@uow.edu.au

Numerical Modelling of Track Behavior Capturing Particle Breakage under Dynamic Loading

Numerical Modelling of Track Behavior Capturing Particle Breakage under Dynamic Loading

Trung Ngo, Ph.D, M.ASCE[1], and Buddhima Indraratna, Ph.D, F.ASCE[2]

[1]ARC Training Centre for Advanced Technologies in Rail Track Infrastructure (ITTC-Rail), Centre for Geomechanics and Railway Engineering (CGRE), University of Wollongong Australia, Northfields Ave, Wollongong NSW 2522; e-mail: trung@uow.edu.au

[2]ARC Training Centre for Advanced Technologies in Rail Track Infrastructure (ITTC-Rail), Centre for Geomechanics and Railway Engineering (CGRE), University of Wollongong Australia, Northfields Ave, Wollongong NSW 2522; e-mail: indra@uow.edu.au

ABSTRACT

This paper presents a study on ballasted track behavior, capturing particle breakage under dynamic loading using large-scale laboratory testing, supplemented with computational modeling approaches. Four large-scale triaxial tests are conducted to investigate the ballast breakage responses subjected to cyclic loading subjected to varying frequencies, f=10-40Hz. Measured laboratory observations show that an increase in loading frequency and magnitude results in significantly increased degradation (breakage) and deformation of ballast. Computational modeling using a coupled discrete-continuum approach (coupled DEM-FEM) is introduced to provide insightful understanding of the deformation and breaking of ballast under cyclic loading. Discrete ballast grains are simulated by bonding of many cylinders together at appropriate sizes and locations. Selected elements located at corners, surfaces and sharp edges of the simulated particles are connected by parallel bonds; and when those bonds are broken, they are considered to represent ballast breakage. The predicted axial strain ε_a, volumetric strain ε_v obtained from the coupled DEM-FEM model agree reasonably well with those observed experimentally. The coupled model is then used to investigate micromechanical aspects of ballast aggregates including the evolution of particle breakage, contact force distributions and orientation of contacts during cyclic loading.

INTRODUCTION

In Australia and around the world, the lack of capacity of rail infrastructure to withstand increased freight volumes and its efficient mobility at high speeds is of grave concern. With vast distances and an export economy based on moving minerals and agricultural goods, designing cost-effective, reliable and well maintained railways is of the utmost importance to Australia's future prosperity. There is an imperitive need to construct railway tracks capable of operating trains that can run at higher speed, bringing a vast challenge to track stability and increased passenger comfort, apart from load bearing capacity of track substructures. The ballast layer is a decisive component of the

conventional track substructure. However, upon repeated wheel loads, ballast deteriorates and spreads laterally which adversely affects the safety and efficiency of railway tracks (Huang et al. 2009, Indraratna et al. 2011, Tutumluer et al. 2012, Ishikawa et al. 2011, Ngo et al. 2017a). Additionally, impact forces induced by wheel defects, rail irregularities and variations in the track foundation conditions (e.g. at stiffness transition zones, such as bridge approaches, road crossings and tunnels) may lead to exacerbated track degradation and more frequent maintenance cycles (Selig and Waters 1994; Le Pen and Powrie 2011, Indraratna et al. 2016, Navaratnarajah et al. 2018). Field measurements are often favored to understand behavior of rail ballast. However, there are many factors and variables including loading and boundary conditions that are often difficult to control in the field (Powrie et al. 2007). Therefore, large-scale laboratory tests simulating as accurately as possible the field loading and boundary conditions are pertinent to obtain realistic ballast stress-strain (deformation) and degradation behavior of rail ballast (Abadi et al 2019, Indraratna and Ngo 2018, Jayasuriya et al. 2019).

A continuum-based modeling methodology has been traditionally used to model railway track embankments. However, owing to the discrete characteristics of ballast grains, the continuum approach is not a feasible approach to accurately capture the micromechanic characteristics of ballast aggregates, including angularity, particle breakage, fabric evolution upon cyclic loading. Meanwhile DEM (discrete element method) has been increasingly used as an alternative to the continuum-based method for investigating of granular and discrete materials (Jiang et al. 2005, Zhang et al. 2016, 2019). The DEM was initially introduced by Cundall and Strack (1979) has been widely used to examine mechanical behavior of ballasted tracks (Cui and O'Sullivan 2006; McDowell *et al*. 2006; Tutumluer *et al*. 2012; Ngo *et al*. 2014; among others). The DEM enables to investigate insight into the micromechanics characteristics of ballast grains that are unlikely to measure experimentally (Indraratna *et al*. 2014, McDowell and Li 2016, Ngo et al. 2017b). A series of large-scale cylindrical dynamic triaxial apparatus was carried out in this study to examine ballast deformation and breakage under varying loading frequencies. A coupled discrete-continuum modeling approach was adopted to simulate a prototype triaxial laboratory tests for ballast assemblies.

LABORATORY TRIAXIAL TESTING

A large-scale cylindrical dynamic triaxial testing apparatus (Fig. 1a) that can incorporate a ballast specimen of 300 mm in diameter and 600 mm high was used in laboratory. The triaxial apparatus consists of five main parts: a triaxial chamber surrounding the membrane and enclosed ballast sample, a high frequency test rig (up to 60 Hz load frequency), a confining pressure system using both compressed air and water where testing can be carried out under relatively low confining pressures typically prevailing in ballast tracks, as well as under high confining pressures (100 kPa) for testing rockfills for other geotechnical applications. A cylindrical rubber membrane (7mm thick) was used to assemble the ballast specimen.

Materials and testing program

Clean basalt was used as ballast aggregates in this study because of its relatively high compressive strength, resistance to weathering and hardness. The ballast was washed and painted in different colors (Fig. 2a) to help distinguish and quantify ballast breakage after the testing. Ballast grains were mixed thoroughly according to the ballast gradation shown in Figure 2c. Sandy-soil was used for subgrade and compacted to a unit weight of 18.5 kN/m^3, followed by a 100 mm-thick compacted capping layer (crushed basalt mixed with sand) to a unit weight of 20.5 kN/m^3. The first layer of ballast (100 mm thick) was placed into the cell membrane overlying the capping and compacted to achieve a unit weight of 15.5 kN/m^3. This process was repeated for the remaining two layers of ballast until the final height of the sample reached a height of 600 mm. Four cyclic tests were conducted under $q_{cyc,max}$ =230 kPa and $q_{cyc,min}$ =30 kPa, subjected to 4 frequencies of f = 10, 20, 30 and 40 Hz and carried out to number of load cycles, N=500,000. During the tests, the axial strain, ε_a and volumetric strain, ε_v were recorded by the linear variable differential transformer (LVDT) and volume change unit (Fig. 1b). The volumetric strain is measured by a device (volumenometer) that has a piston located coaxially within a small cylindrical chamber connected to the cell. The smooth piston moves upward or downward depending on volume increase or decrease. The ballast grains were sieved after test, and the changes in particle size were recorded to analyze the extent of breakage.

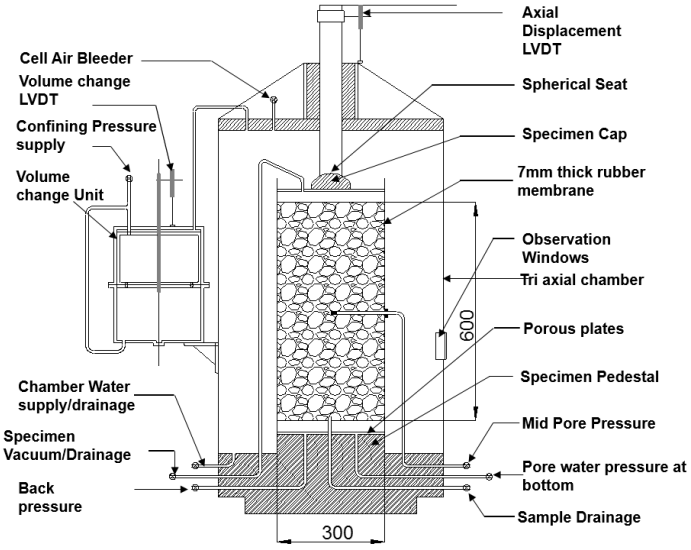

(a) (b)

Figure 1. (a) large-scale triaxial apparatus; and (b) cross section of the apparatus

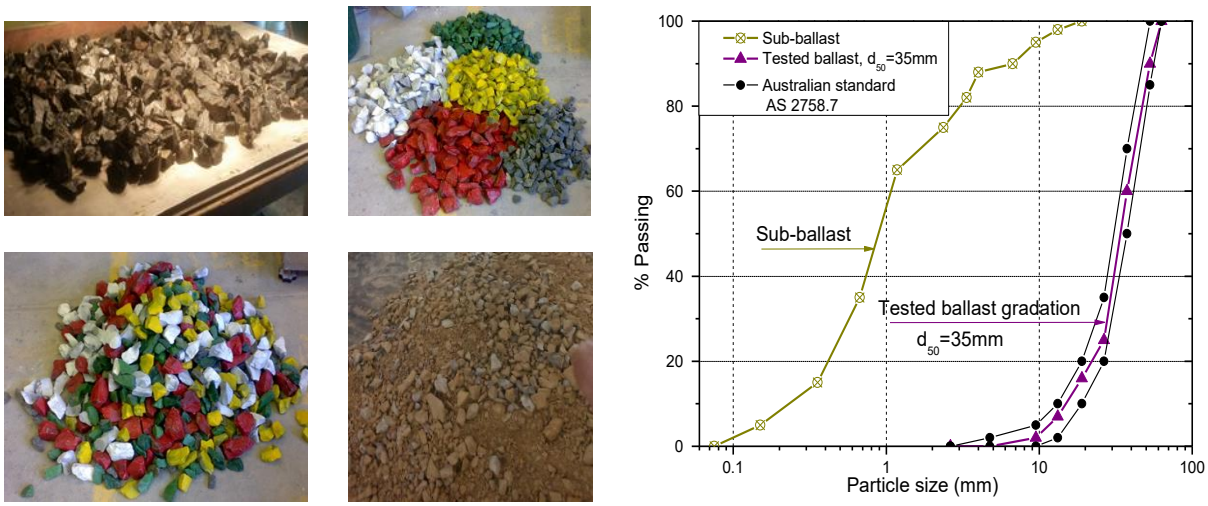

Figure 2. a) Ballast and capping tested; (b) Particle size distribution of tested materials

Figure 3 presents the measured axial strain, ε_a and volumetric strain, ε_v with load cycle, N under a range of loading frequencies, f=10-40 Hz. It is seen that ε_a increases with an increase in N and higher the frequency, f produced the greater ε_a. There is a definite trend of increasing axial strain within the first thousand load cycles, followed by a gradual increase of the ε_a at a decreasing rate (Fig. 3a). In fact, when the aggregates were compressed to a threshold packing arrangement, subsequent loading would initiate volumetric dilation and particle breakage. Measured volumetric changes ε_v increases with an increase of frequency (f). All specimens showed significant volumetric compression at initial loading cycles (N=1000), followed by a decreasing rate of compression at subsequent loading cycles. Tests carried under low frequencies of f=10, 20 Hz show volumetric compression throughout the tests. On the other hand, under frequencies of f=30 and 40 Hz ballast shows a dilative response after N=10,000 cycles. Some of the test data is used in this study to validate a coupled DEM-FEM model.

COUPLED DISCRETE-CONTINUUM ANALYSIS

The aggregates were simulated in 2D DEM through developed subroutines, capturing the angularity of ballast aggregates, utilizing commercial software PFC2D, Itasca (2016). Underlying capping and subgrade layers were simulated by the continuum method (FEM). Interface elements were introduced to facilitate the coupling process between the DEM and FEM. Ballast grains were simulated in DEM by bonding many cylinders together at predetermined size and locations (Fig. 4a). The breaking of these bonds was considered to represent ballast breakage. Micro-mechanical parameters for ballast grains used in DEM analysis were determined by calibration with laboratory test data. Due to the brevity of this paper, details of model calibration and validation are not presented, but it is noted in this study the experimental and DEM models reasonably agree in terms of axial and volumetric strains. Figure 4b shows a schematic diagram of a coupled discrete-

continuum (DEM-FDM) model, where the subgrade and capping were simulated by the continuum approach. The capping and subgrade were simulated as an elasto-plastic material following the Mohr-Coulomb yield criterion and material parameters (Young's modulus E, Poison's ratio ν, cohesion c, friction angle ϕ, and dilatancy angle ψ) were determined earlier in the laboratory. Interaction between ballast grains (Zone 1) and capping (Zone 2) was by transferring of contact forces and displacements between the two domains (Fig. 4c). The schematic diagram of exchanging of contact forces (F_n, F_s) and velocity ($\dot{X}_i^{[E]}$) between the discrete particles and continuum elements at their interfaces is presented in Figure 4d. The superscripts *C*, *E*, and *P* represent contact, element, and particle, respectively.

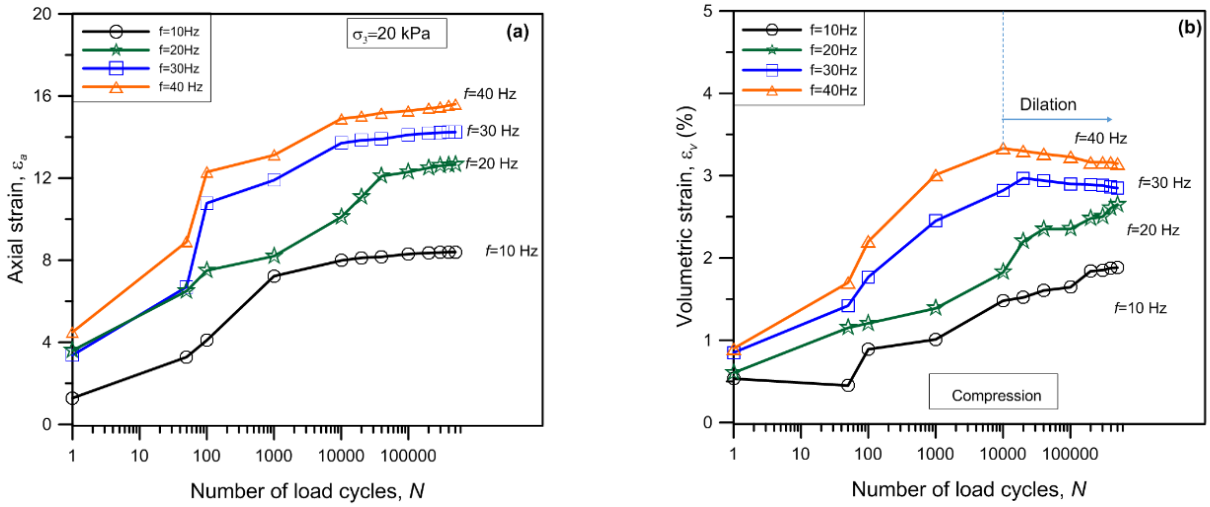

Figure 3. Measured responses of ballast subjected to varying loading frequencies, *f*=10-40: (a) axial strain, ε_a ; and (b) volumetric strain, ε_v

Contact forces at the interface are computed as:

$$F_i^{[C]} = F_n^{[C]} + F_S^{[C]} \tag{1}$$

where, contact normal force ($F_n^{[C]}$) and increment of shear force ($\Delta F_s^{[C]}$) are calculated by:

$$F_n^{[C]} = K^n U^n n_i \;; \quad \text{and} \quad \Delta F_s^{[C]} = -K^s \left(\Delta X_i^{[C]} - \Delta X_i^{[C]} n_i \right) \tag{2}$$

The resultant forces and moments acting on particles at the interface are given by:

$$F_i^{[P]} \leftarrow F_i^{[P]} - F_i^{[C]}; \text{ and } M_i^{[P]} \leftarrow M_i^{[P]} - e_{ijk} \left(X_j^{[C]} - X_j^{[P]} \right) F_k^{[C]} \tag{3}$$

The relative contact velocity (i.d. displacement) at the interface (V_i) is determined by:

$$V_i = \dot{X}_{i,E}^{[C]} - \dot{X}_{i,E}^{[P]} = \dot{X}_{i,E}^{C} - \left[\dot{X}_i^{[P]} + e_{ijk} \omega_j^{[P]} (X_k^{[C]} - X_k^{[P]}) \right] \tag{4}$$

where, $\dot{X}_{i,E}^{[C]}$ and $\dot{X}_{i,E}^{[P]}$ are the velocities of element and particle, respectively. $\dot{X}_i^{[P]}$ and $\omega^{[P]}_j$ are translational and rotational of the particle, and e_{ijk} is the permutation symbol.

The velocity of continuum elements at the interface (i.e. displacement) is then determined by:

$$\dot{X}_{i,E}^{[C]} = \sum N_j \dot{X}_{i,E}^{j} \tag{5}$$

where, N_j is a shape function, given by: $N_j = (1+\xi_o)(1+\eta_o)/4$, $j = 1,2,3,4$; and $\xi_o = \xi_i \xi$, $\eta_o = \eta_i \eta$; ξ_i and η_i are local coordinates of nodes. At the interface, the shear and the normal contact forces are distributed to the nodal force, $F_i^{[E,j]}$ following to the shape function N_j, given by: $F_i^{[E,j]} = F_i^{[E]} + F_i^{[C]} N_j$ (6)

The exchange of force-displacement was implemented by interface elements, and a mathematical framework was formulated to distribute forces and moments to nodal points (Fig. 4d) is governed by a parameter, Θ (Indraratna et al. 2015), as given by:

$$\Theta = \frac{M - F_Y \times (X_B - X_C) + F_X \times (Y_B - Y_C)}{F_Y \times (X_A - X_B) - F_X \times (Y_A - Y_B)} \tag{1}$$

Simulated ballast breakage

Ballast particles were simulated by bonding of cylinders together using contact bonds. If stresses acting on these bonds exceed its corresponding strength, the bond breaks; and the breaking of these bonds within a simulated particle is considered to represent particle breakage (B_r). Amount of broken bonds B_r predicted from the coupled DEM-FEM analysis is presented in Figure 5a. The coupled model was carried out under four frequencies of f=10-40 Hz subjected to N=10,000 cycles; and the accumulation of bond breaking increased load cycle, N; and this trend is similar to those of BBI measured from the laboratory testing (Sun *et al.* 2018). It is noted that particle breakage causes a shift in the initial particle size distribution (PSD) towards smaller particle sizes. The BBI is then determined by sieving the ballast before and after every test and then quantifying the differences in areas of particle size distribution curves (Indraratna and Ngo 2018). At a given frequency, the amount of bond breakage increases significantly within the first N = 5,000 cycles; and then remains relatively constant at subsequent loading cycles. It is noted that while the BBI increases with an increase of load cycle, the predicted B_r shows almost plateau after 6000 cycles. This is a limitation of 2D DEM simulations carried out in this study that did not capture correct angularity and irregular shape of ballast aggregates.

Typical snapshots of breaking bonds (representing ballast breakage) captured from simulations under a given frequency of f=20 Hz is illustrated in Figure 5b. It shows that the amount of bond breakages increases with increased load cycles. Within the first N=1000 cycles, the majority of the broken bonds appears right below the top loading plate. There is an increase in particle breakages at subsequent loading and they distribute across the ballast assembly.

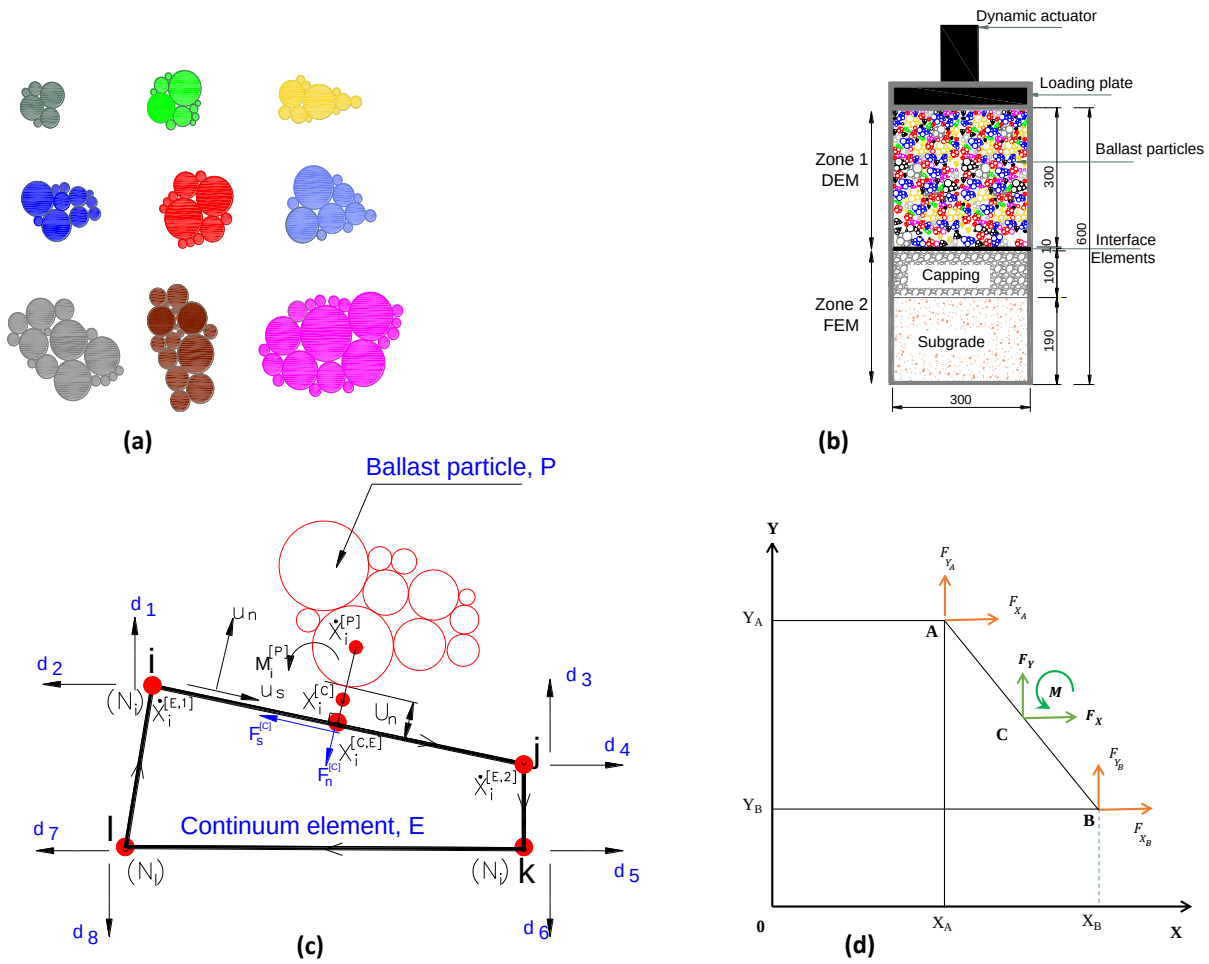

Figure 4. (a) simulated ballast grains; (a) coupled DEM-FEM model; (c) interaction of a discrete grain with continuum element; and (d) transfer of forces and moments

Contact force distributions

Figure 6 illustrates the evolutions of contact forces of the ballast assembly together with vertical stress contours in the capping and subgrade layers at different load cycles of N=100, 1000, 5000 and 10,000 cycles under a given frequency of f=20 Hz. It is observed that the applied cyclic loads are transmitted to discrete grains in a form of contact force-chains where each contact force is represented at the contact point having a thickness proportional to the intensity of the forces. Contact forces in the DEM domain are heterogeneous, where the maximum contact forces change with load cycles. Initially, large contact forces occurred and concentrated beneath a top-loading plate, and around wall edges. Compressive stresses in the capping and subgrade are high around the interface regions with the particles, whereby they are predicted to decrease with depth. An increase in number of load cycles results in an increased number of contacts and greater contact force magnitudes. This is attributed to the densification of the sample and governed by the re-arrangement and breaking of particles.

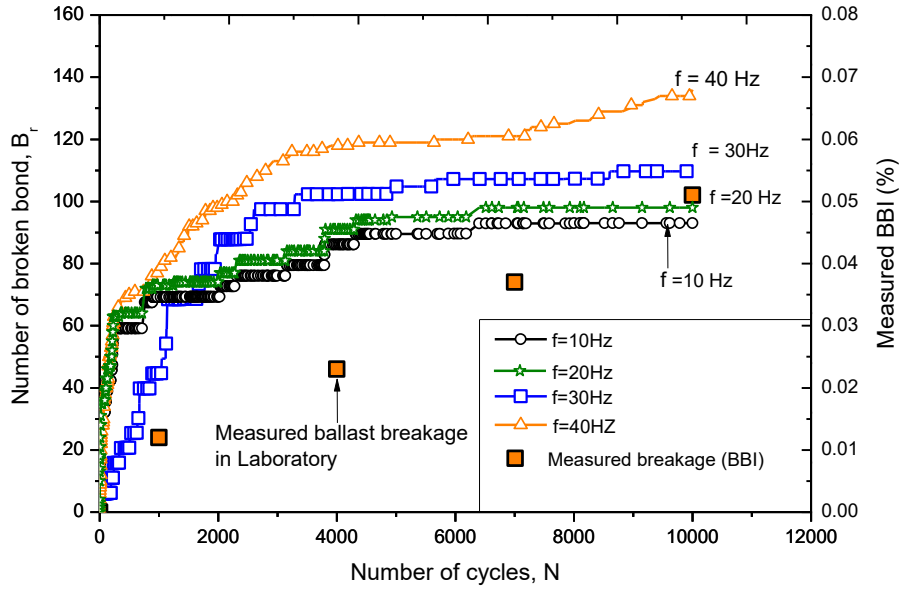

(a)

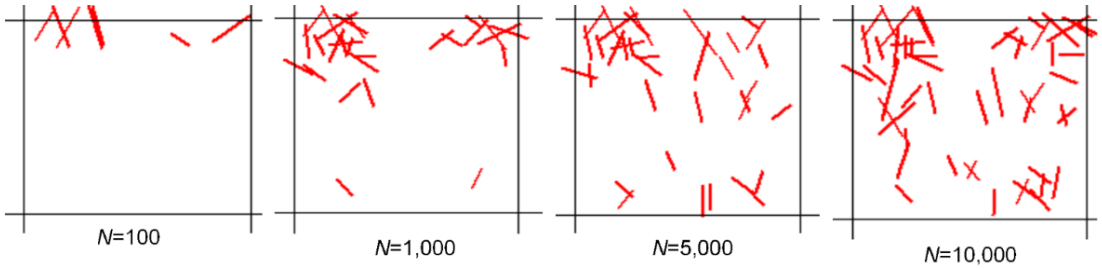

(b)

Figure 5. (a) Evolutions of contact bond broken; and (b) Snapshots of breaking bonds

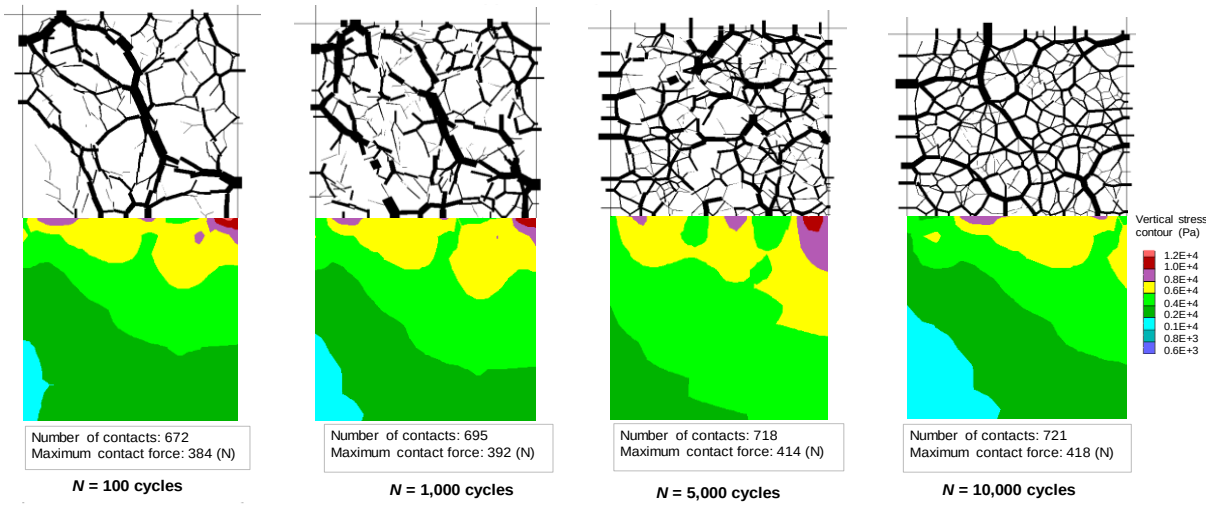

Figure 6: Contact force distributions in ballast and stress contour in the capping/subgrade.

CONCLUSIONS

This paper presented results measured from large-scale cyclic triaxial tests and coupled discrete-continuum modeling for railway ballast. Four tests were conducted subjected to a given $q_{cyc,max}$ =230 kPa, $q_{cyc,min}$ =30 kPa under varying cyclic loading frequencies, f= 10, 20, 30 and 40 Hz and carried out up to N=500,000 load cycles. A coupled DEM-FEM was established and applied in simulating cyclic triaxial tests and results of shear stress-strain responses obtained from simulations were comparable with those measured in laboratory. The coupling model was used to predict the number of bond breaking (ballast breakage) and it demonstrated that the broken bonds increased with increased frequency. Contact force distributions were also examined, and they indicated that the contact forces distributed non-uniformly across the ballast assembly. Results obtained from this study could provide more insight into the micromechanical responses and contact forces transmitted in a ballast assembly.

ACKNOWLEDGEMENTS

This study was carried out by the ARC- Industrial Transformation Training Centre for Advanced Technologies in Rail Track Infrastructure (IC170100006) and funded by the Australian Government (ITTC-Rail). The support of colleague A/Prof Cholachat Rujikiatkamjorn, A/Prof Jayan Vinod, Dr Ana Heitor and CME-technicans are appreciated.

REFERENCES

Abadi, T., Pen, L.L., Zervos, A. and Powrie, W. (2019). Effect of Sleeper Interventions on Railway Track Performance. *J of Geotech and Geoenvir Eng*, 145(4), 04019009.

Cui, L. and O'Sullivan, C. (2006). Exploring the macro- and micro-scale response of an idealised granular material in the direct shear apparatus. *Geotechnique*, 56(7), 455-468.

Cundall, and Strack, O. (1979). A discrete numerical model for granular assemblies. *Geotechnique*, 29(1), 47-65.

Huang, H., Tutumluer, E. and Dombrow, W. (2009). "Laboratory characterisation of fouled railroad ballast behavior." *Transportation Research Record: No. 2117*, Washington, DC.

Indraratna, B., Ngo, N.T. and Rujikiatkamjorn, C. (2011). Behavior of geogrid-reinforced ballast under various levels of fouling. *Geotextiles and Geomembranes*, 29(3), 313-322.

Indraratna, B., Ngo, N.T., Rujikiatkamjorn, C. and Vinod, J. (2014). Behaviour of fresh and fouled railway ballast subjected to direct shear testing - a discrete element simulation. *Int J Geomech*, 14(1), 34-44.

Indraratna, B., Ngo, N.T., Rujikiatkamjorn, C. and Sloan, S.W. (2015). Coupled discrete element–finite difference method for analysing the load-deformation behaviour of a single stone column in soft soil. *Computers and Geotechnics*, 63, 267-278.

Ishikawa, T., Sekine, E. and Miura, S. (2011). Cyclic deformation of granular material subjected to moving-wheel loads. *Canadian Geotechnical Journal*, 48(5), 691-703.

Indraratna, Nimbalkar, Ngo, T. Neville. (2016). Performance improvement of rail track substructure using artificial inclusions – Experimental and numerical studies. *Transportation Geotechnics*, 8, 69-85.

Indraratna, B. and Ngo, T. (2018). Ballast Railroad Design: Smart-Uow Approach, CRC Press.

Itasca (2016). Particle flow code (PFC2D). Itasca Consulting Group, Inc., Minnesota.

Jiang, M.J., Yu, H.S. and Harris, D. (2005). A novel discrete model for granular material incorporating rolling resistance. *Computers and Geotechnics,* 32, 340–357.

Jayasuriya, C., Indraratna, B. and Ngo, T.N. (2019). Experimental study to examine the role of under sleeper pads for improved performance of ballast under cyclic loading. *Transportation Geotechnics,* 19, 61-73.

Le Pen, and Powrie, W. (2011). Contribution of Base, Crib, and Shoulder Ballast to the Lateral Sliding Resistance of Railway Track. *Journal of Rail and Rapid Transit*, 225(2), 113-128.

McDowell, G.R. and Li, H. (2016). Discrete element modelling of scaled railway ballast under triaxial conditions. *Granular Matter*, 18(3), 66.

Navaratnarajah, S.K., Indraratna, B. and Ngo, N.T. (2018). Influence of under sleeper pads on ballast behavior under cyclic loading: experimental and numerical studies. *Journal of Geotechnical and Geoenvironmental Engineering*, 144(9), 04018068.

Ngo, N.T., Indraratna, B. and Rujikiatkamjorn, C. (2014). DEM simulation of the behaviour of geogrid stabilised ballast fouled with coal. *Computers and Geotechnics*, 55, pp: 224-231.

Ngo,T., Indraratna and Rujikiatkamjorn. (2017a). A study of the geogrid–subballast interface via experimental evaluation and discrete element modelling. *Granu. Matter*, 19(3), 51-16.

Ngo, N.T., Indraratna, B. and Rujikiatkamjorn, C. (2017b). Simulation Ballasted Track Behavior: Numerical Treatment and Field Application. *Int J Geomech*, 17(6), 04016130.

Powrie, W., Yang, L.A. and Clayton, C.R.I. (2007). Stress changes in the ground below ballasted railway track during train passage. *Journal of Rail and Rapid Transit*, 247-261.

Selig, E.T. and Waters. (1994). Track geotechnology and substructure management, Telford.

Sun, Q., Indraratna, B. and Ngo, N.T. (2018). Effect of increase in load and frequency on the resilience of railway ballast. *Géotechnique*, DOI: https://doi.org/10.1680/jgeot.17.P.302.

Tutumluer, E., Huang, H. and Bian, X. (2012). Geogrid-aggregate interlock mechanism investigated through aggregate imaging-based discrete element modeling approach. *Int J Geomech*, 12(4), 391-398.

Zhang, Zhao, and Zhai, W. 2019. Importance of load frequency in applying cyclic loads to investigate ballast deformation under high-speed train loads. *Soil Dynamics and Earthquake Engineering*, *120*, pp.28-38.

Zhang, Zhao, Zhai, 2016. Dynamic behavior analysis of high-speed railway ballast under moving vehicle loads using discrete element method. *Int J Geomech, 17*(7),04016157.